

# A Reduced-Order Mud Reaction Force Model for Robotic Foot-Mud Interactions

Xunjie Chen, Jingang Yi, and Jerry Shan

**Abstract**—Legged robots are well-suited for broad exploration tasks in complex environments with yielding terrain. Understanding robotic foot-terrain interactions is critical for safe locomotion and walking efficiency for legged robots. This paper presents a reduced-order mud reaction force model (MRF) for robotic foot-mud interactions. We focus on vertical robot locomotion on mud and propose a visco-elasto-plastic analog to model the foot-mud interaction forces. Dynamic behaviors such as mud visco-elasticity, withdrawing cohesive suction, and yielding are explicitly discussed with the proposed model. Besides comparing with dry/wet granular materials, mud intrusion experiments are conducted to validate the force model. The dependency of the model parameter on water content and foot velocity is also studied to reveal in-depth model properties under various conditions.

## I. INTRODUCTION

Although legged robots are attractive and well-suited for exploration tasks, it is still challenging to guarantee the rapid and safe locomotion of legged robots on deformable and multifaceted terrains [1], [2]. Recent study of robot locomotion has mainly focused on dry granular terrain (e.g., sand) using the resistive force theory (RFT) [3], [4], digging/burrowing strategies [5], [6] and walking locomotion [7], [8]. However, legged locomotion on yielding terrain such as muddy ground is rarely investigated. In [9], an immersed pulling scenario through wet granular packing was considered. The Darcy-flow mechanism and a one-dimensional visco-elastic-plastic drag-force model were applied to interpret experimental observations and infer underlying physics.

Unlike granular materials, mud rheology is highly sensitive to clay type and solid concentration level. It is challenging to predict the foot-mud interaction force from its ingredient components [10]. Rigorous constitutive models for mud rheology such as Herschel-Bulkley (HB) models [11] were used to describe mud flow curves, that is, the relationships among shear stress and shear rate. A new contribution of constitutive equation in [12] was proposed to combine “Bingham” model and the model in [11]. Another new viscoelastic thixotropic model in [13] used a parallel combination of an infinite shear viscosity damper with a viscoelastic Maxwell model to explain mud rheology.

The above-mentioned fundamental constitutive models cannot however be directly applied to study robotic foot-mud interactions because it is difficult to estimate and obtain accurate shear rate of mud microstructure in real time. Detailed understanding of the relationship between

robot locomotion and mud rheological responses is still missing. Legged flipper robots were previously studied on muddy terrain [14], [15]. In [15], two featured locomotion failure mechanisms were discussed and related to mud water content. Several useful observations of vertical intrusions on mud were presented for force hysteresis, suction force as well as energy consumption perspectives under different mud conditions (e.g., water content) [16]. However, the qualitative relationships between peak (suction) force and stepping locomotion velocity, water content, and foot shapes are still unclear. It is also challenging to estimate reaction forces for potential locomotion gait optimization by only sensing robot motion information (e.g., velocity and acceleration).

We present a mud reaction force (MRF) model for foot-mud interactions in robotic locomotion. We conduct one-dimensional (1D) mud intrusion experiments to obtain mud-reaction-force characteristics such as relaxation time, cohesive suction force, and hysteresis. A reduced-order model is then proposed using a visco-elasto-plastic mechanical analog. The model considers both dynamic intrusion and withdrawal (when suction happens) processes given a robot locomotion input. We conduct experiments to estimate the model parameters and validate the model accuracy. The dependency of the model parameters on the locomotion velocity and mud properties (i.e., water content) is also discussed as a fundamental case study. The main contribution of this work are twofold. First, the proposed MRF model for robotic foot-mud interactions is new. The model directly predicts mud rheological response rather than through solving constitutive equations and therefore, enables potential use to develop a real-time force estimation and robot control. Second, this model presents a uniform, compact formulation for both the foot intrusion and withdrawn motions, describing the force-generation mechanism and including mud cohesion/suction with only a few parameters. These features are attractive for further usage in robot dynamics and control.

## II. ONE-DIMENSIONAL FOOT-MUD INTERACTIONS

We focus on one-dimensional (1D) mud-resistive-force modeling, and therefore, a series of 1D mud-penetration experiments were performed with a prescribed mud formulation and experimental protocols. Fig. 1(a) shows the experimental setup. All mud intrusion experiments were conducted within a container with a size of  $28 \times 23 \times 15$  cm. We filled the container with customized mud mixtures. The mixed mud materials included controlled volume of clay (Sea Mix 6 from Seattle Pottery Supply), sand (150-600  $\mu\text{m}$  graded standard silica sand from Gilson Inc.), and water in certain

X. Chen, J. Yi, and J. Shan are with the Department of Mechanical and Aerospace Engineering, Rutgers University, Piscataway, NJ 08854 USA (email: xc337@rutgers.edu, jyji@rutgers.edu, jshan@soe.rutgers.edu).

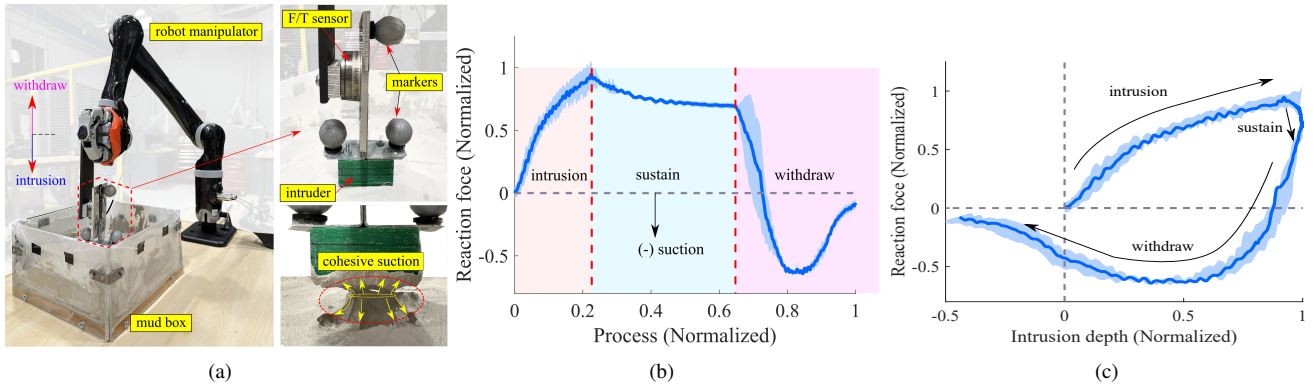


Fig. 1. (a) Mud-intrusion experimental setup with a cuboid intruder. The necking of mud that leads to a cohesive suction force during the withdrawal process. (b) (c) A typical resistive-force profile (normalized) in normalized process (time) domain and in normalized intrusion-depth domain, respectively. Shaded regions demonstrate one-standard deviation from 3 trials.

proportion. For all reported data, we set the clay-to-sand ratio as 3:1 in all cases. We used volume ratio to define the water content of muddy mixtures. By changing the water content, denoted by  $W$ , rheological (related to deformation and yield stress) properties of mud can be controlled. We used a 3D-printed cuboid (with size of  $51 \times 38 \times 25$  mm) as the intruder and the face  $51 \times 38$  mm is facing downward the ground for all intrusion tests.

To implement 1D motion along the vertical direction, the intruder was mounted at the end-effector of a robotic manipulator (Jaco from Kinova Inc.) to move downward and upward. Optical markers and a motion-capture system (10 Bonita cameras from Vicon Ltd.) were used to obtain the real motion of the intruder. A 3-axis force/torque (F/T) sensor (model mini45 from ATI Inc.) was used to measure the resistive forces during the penetration motion.

For a single intrusion test under a certain water content, the intruder first moved downward and vertically with a prescribed constant velocity until reaching at a certain designed intrusion depth. We then maintained the intruder position temporarily to let the reaction force become stable within a time interval (6 s). Finally, we withdrew the intruder upward with the same velocity as the intrusion process until it totally separated away from clinging mud. Both force and motion data were synchronized and recorded with the 100 Hz sampling frequency. For each water-content level and intrusion/withdrawing velocity condition, three trials were repeated, with the mud surface flattened before each trial. We intentionally did not immerse the intruder completely into the mud because we tried to exclude any additional force due to any mud on the top. Through this motion, we captured the natural relaxation characteristics at a sustained intrusion depth, and emphasized the cohesive suction force between the mud and the bottom contact surface of the intruder upon withdrawal, rather than the resistive weight induced by materials on top.

Fig. 1(b) shows the result of the reaction force in experiments. The reaction force experienced three stages: intrusion increasing, sustain, and withdrawing suction regimes. Fig. 1(c) shows the reaction force versus the intrusion displacement, which was normalized by the final depth. Unlike the almost linear stiffness mentioned for the granular

materials [3], a nonlinear hysteresis was observed during entire intrusion and withdrawal processes. It is also noted that the reaction force during the sustain part of the process decayed gradually to a steady value as shown in Fig. 1(b) due to the natural visco-elasticity of mud under a given applied force (stress). A clear force (stress) relaxation was observed and this relaxation time is assumed to be only related to material characteristics such as clay-to-sand ratio and water content.

As the intruder withdrew, the reaction force dropped rapidly and crossed zero before becoming negative and creating a suction under the intruder. Fig. 1(a) illustrates the cohesive property and plastic deformation (necking) of mud. The necking effect provides a suction force pulling the intruder downwards, which is a particular feature for foot-mud interactions. Generally, the suction drops if the internal stress goes beyond the fracture limit of the mud. Nevertheless, the pulling force (magnitude) decays slowly, and therefore, less weight pulls down on the intruder.

Based on aforementioned insights, we conclude that non-linear modeling should be considered for both intrusion and withdrawal processes. Moreover, an ideal force model should cover all the three intrusion regimes.

### III. REDUCED-ORDER MUD RESISTIVE FORCE MODEL

Instead of modeling mud complex physical behavior, we present a reduced-order model based on a combination of elementary mechanism. Fig. 2 illustrates the schematics of the intruder-mud interaction modeling by a visco-elasto-plastic mechanism for both the penetration and withdrawal processes. The intruder moves penetrating into (downward) and pulling out (upward) of mud. Since there is no mud on the upper surface of the intruder, the resistive force only comes from the bottom and side interaction. The reaction force is considered uniform across the surface in contact with mud and then the total reaction force is calculated as  $F = f_m S$ , where  $f_m$  is the resultant mud force and  $S$  is the total contact area.

1) *Intrusion modeling*: Fig. 2(a) illustrates the intrusion process when the intruder moves downward in mud. The model comprises a Maxwell visco-elastic element [9], [13], a frictional slider, and another elastic element that is connected

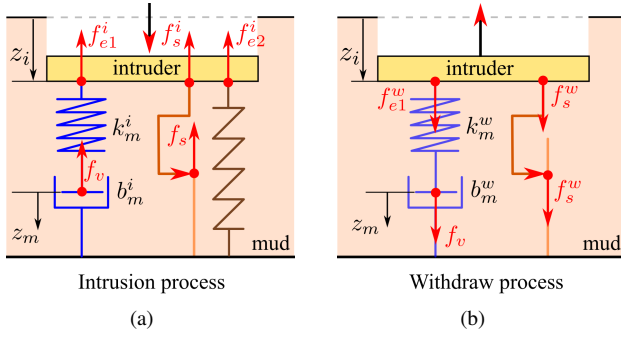


Fig. 2. Schematics of 1D foot/mud interaction models using combinations of visco-elasto-plastic elements for (a) Intrusion and (b) Withdrawal process.

in parallel. We consider mud substrate as a visco-elastic element producing the micro-elastic deformation for the mud internal action. Its resultant stress applied to the intruder is denoted by  $f_{e1}^i$ . The single spring element produces a resistive stress, denoted by  $f_{e2}^i$ , due to the macroscopic (bulk) deformation of the mud material enforced by the motion of the intruder. Finally, the additional slider contributes a viscous frictional stress, denoted by  $f_s^i$ . The resultant resistive stress applied to the intruder is

$$f_m^i = f_{e1}^i + f_{e2}^i + f_s^i. \quad (1)$$

We use superscript “i” to represent the force during the intrusion process. Denoting the penetration displacement of the intruder originating from the mud surface as  $z_i$  and the internal displacement of mud substrates as  $z_m$ , we obtain the elastic stress  $f_{e1}^i$  and viscous damping stress  $f_v^i$  as

$$f_{e1}^i = k_m^i (z_i - z_m), \quad f_v^i = b_m^i \dot{z}_m, \quad (2)$$

where  $k_m^i$  and  $b_m^i$  represent the stiffness and damping coefficients for the mud, respectively. For the internal force balance, we have  $f_{e1}^i = f_v^i$  and therefore, from (2) we obtain

$$b_m^i \dot{z}_m + k_m^i z_m = k_m^i z_i. \quad (3)$$

The initial conditions are  $z_m(0) = \dot{z}_m(0) = 0$ . Given  $z_i$ , from (3) we update  $z_m$  and use (2) to obtain force  $f_{e1}^i$ .

Considering the resistance of the instantaneous volume change, force  $f_{e2}^i$  inferred by a single nonlinear spring is

$$f_{e2}^i = \alpha \left( \frac{z_i}{H} \right)^\beta, \quad (4)$$

where  $\alpha$  is defined as the stiffness related to direct volume change of mud,  $\beta \in (0, 1]$  is a constant, and  $H$  is the intruder width. Viscous friction force  $f_s^i$  is considered as inertial drag at a regime where force magnitude increases quadratically with motion velocity [17], and therefore,

$$f_s^i = \text{sign}(\dot{z}_i) \lambda \rho_m \dot{z}_i^2, \quad (5)$$

where  $\rho_m$  is the mass density of mud,  $\lambda$  is scaling factor determined by calibration and function  $\text{sign}(x) = 1$  for  $x \geq 0$  and  $-1$  otherwise.

2) *Withdrawing and beyond-necking modeling*: Suction force was observed during the withdrawal, and we suppose that this suction force comes from the cohesiveness of the mud as well as its viscosity due to the internal presence of water. Fig. 2(b) shows the schematic of the withdrawing force model. We do not consider the resistance due to significant volume deformation. Therefore, the total reaction stress is,

$$f_m^w = f_{e1}^w + f_s^w,$$

where we use superscript “w” to represent the force during the withdrawal process. The visco-elastic force  $f_{e1}^w = k_m^w (z_i - z_m)$  and viscous friction force  $f_s^w$  is calculated similar to (5). With  $k_m^w$ ,  $b_m^w$ , and we have  $b_m^w \dot{z}_m + k_m^w z_m = k_m^w z_i$  for the withdrawing process.

We denote the mud yield stress by  $\sigma_y$ . When the stress goes beyond  $\sigma_y$ , breakage and collapse of interconnected network of mud flocs would happen [18]. This results in the drop of the suction-force magnitude shown in the later phase in Fig. 1(b). We found that the displacement velocity ( $\dot{z}_m$ ) decayed to zero gradually instead of suddenly stopping deforming in experiments. To capture this behavior, a second-order filter is used to model the mud velocity after necking. The mud velocity follows that  $V_m(s) = G_m(s)v_{m0}$ , where  $V_m(s)$  is the Laplace transformations of mud velocity  $v_m(t) = \dot{z}_m(t)$  after necking and  $v_{m0}$  is the mud velocity before necking. Based on the physical mechanism analog of the spring-damper system as shown in Fig. 2(b), the lumped mud motion without considering intruder motion is  $m\ddot{z}_m + b_m\dot{z}_m + k_m z_m = 0$ . Considering initial conditions that  $z_{m0} = 0$  and  $\dot{z}_{m0} = v_{m0}$  at necking and taking Laplace transformation, we obtain

$$G_m(s) = \frac{s}{s^2 + 2\zeta\omega_0 s + \omega_0^2}, \quad (6)$$

where both  $\omega_0$  and  $\zeta$  are constant parameters related to mud materials. Here  $\omega_0 \propto \sqrt{k_m}$  and  $\zeta \propto \frac{b_m}{\sqrt{k_m}}$ . We set  $v_{m0}(t)$  before necking as the command velocity input to  $G_m(s)$  and step function that drops to zero is used for  $v_{m0}(t)$ .

Fig. 3 shows the flow chart of the proposed mud reaction force model. The motion information of the intruder (i.e.,  $\dot{z}_i$ ) is used as an input to model (3) to estimate the mud displacement  $z_m$  for force calculation. Under the withdrawing condition, we design a yielding/necking switch to regulate the mud displacement velocity as a gradually decaying profile by using the velocity filter

$$G_m(s) = \begin{cases} 1, & |f_m^w| \leq \sigma_y \\ \frac{s}{s^2 + 2\zeta\omega_0 s + \omega_0^2}, & |f_m^w| > \sigma_y. \end{cases} \quad (7)$$

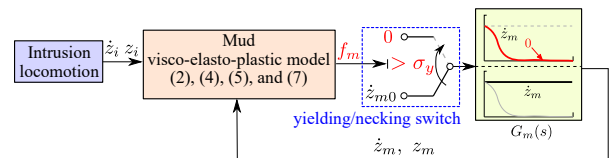


Fig. 3. The MRF model diagram. A switch is used for regulating the mud velocity  $\dot{z}_m$  to interpret necking after significant yielding.

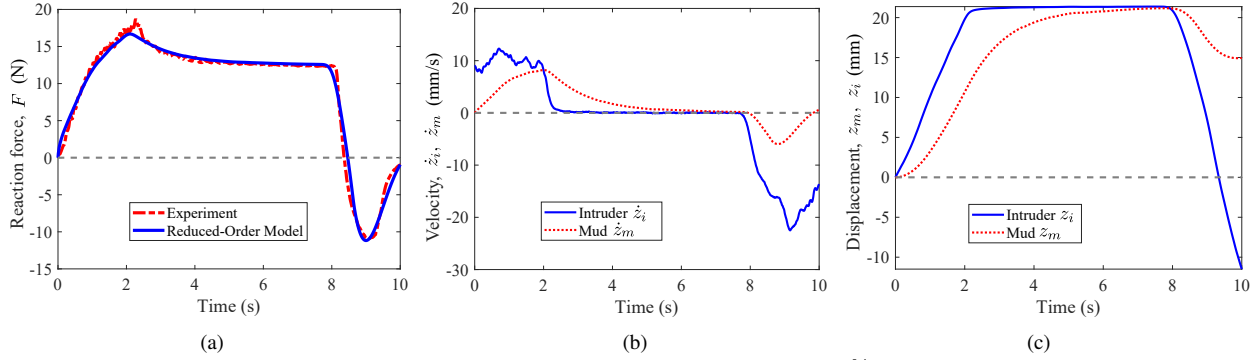


Fig. 5. Mud intrusion experiment and model validation results for mud with water content  $W = 25\%$ . (a) Reaction force experiments and comparison with the model prediction. (b) Recorded intruder velocity  $\dot{z}_i$  and estimated mud velocity  $\dot{z}_m$ . (c) Intrusion displacements  $z_i$  and  $z_m$  for the intruder and mud.

Without yielding/necking, the mud velocity after the filter holds the value before necking, that is,  $\dot{z}_m = \dot{z}_{m0}$ , where  $\dot{z}_{m0}$  ( $\dot{z}_m$ ) represents the mud velocity before (after) the filter. After yielding condition, the mud velocity is enforced to drop to zero, that is,  $\dot{z}_m \rightarrow 0$  when  $|f_m^w| > \sigma_y$ . The values of the yielding strength  $\sigma_y$ , the filter parameters  $\omega_0$  and  $\zeta$ , which depend on water content and mud composition, are obtained by experimental identification.

#### IV. MODEL VALIDATION AND RESULTS

We first calibrated and estimated the mud parameters. The mass density of the synthetic mud is  $\rho_m = 1.84 \times 10^3 \text{ kg/m}^3$  for mud water content  $W = 25\%$ . As  $W$  varied from 15% to 35%, the mud density did not change much since the weight of water contributed not significantly to total mud materials. Therefore, we used the mud density at  $W = 25\%$  as a representation. The sliding experiments were conducted by making the intruder contact the mud surface with a small depth (5 mm) and moving it along one direction. Fig. 4 shows the corresponding calibration results, which gave the scaling constant estimate  $\lambda = 13$ .

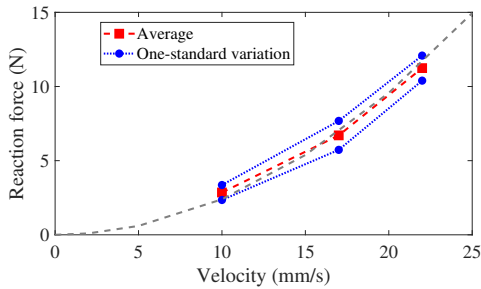


Fig. 4. Calibration result of the scaling factor  $\lambda$ .

For other model parameters, we conducted series of intrusion experiments under different water contents and moving velocities. Calibration was performed by formulating an optimization problem to minimize the difference between the model prediction and the experimental results. Table I lists the values of the estimated model parameters.

We show experimental results under water content  $W = 25\%$  for model validations. Fig. 5(a) shows the model estimation results. The model estimation matched the test results

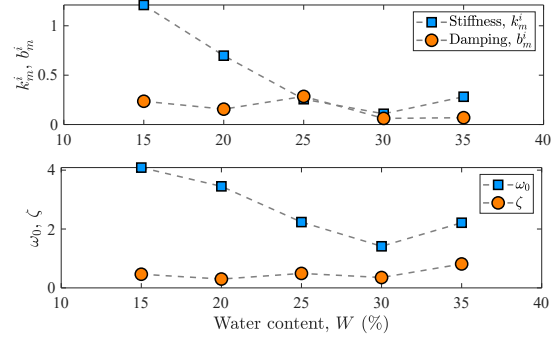


Fig. 6. The dependency of the model parameters  $k_m^i$ ,  $b_m^i$  and filter parameters  $\zeta$ ,  $\omega_0$  on the mud's water content  $W$ .

accurately over the entire intrusion/withdrawing process. Figs. 5(b) and 5(c) further show the velocity and displacement profiles respectively for the intruder and the mud. We evaluated model estimation performance under different water content conditions by using the identified parameter values in Table I. We calculated the relative estimation error as  $e = \Delta F / \max(F_m)$ , where  $\Delta F$  is force difference between model estimation and experimental measurement and  $F_m$  is mud force from load cell measurement. The last column in Table I lists the root mean square error (RMSE) for the average error.

It is found that mud stiffness  $k_m^i$  ( $k_m^w$ ) and damping coefficient  $b_m^i$  ( $b_m^w$ ) are kept consistently under the same experimental condition. Furthermore, the values of parameters  $k_m^w$  and  $b_m^w$  are kept almost constant even for different water content conditions. The top plot of Fig. 6 shows the dependency of the mud stiffness and damping parameters  $k_m^i$  and  $b_m^i$  on water content  $W$ . Below a certain water content level (i.e.,  $W \leq 30\%$ ), mud stiffness value decreases significantly with the increasing water content  $W$ , while damping coefficient values changes only slightly. This observation also agrees with the filter parameters  $\omega_0$ ,  $\zeta$  as shown in the bottom plot of Fig. 6. This is not surprising since  $\omega_0 \propto \sqrt{k_m}$  and  $\zeta \propto b_m$ . Fig. 7 further shows the effects of the water content on the stiffness parameters  $\alpha$ ,  $\beta$ , and threshold  $\sigma_y$ . The stiffness  $\alpha$  and yield stress  $\sigma_y$  decrease significantly as  $W$  increases. With a lower  $W$ , mud creates a substantial

TABLE I  
PARAMETER VALUES FOR MUD WITH DIFFERENT WATER CONTENT AND MODEL ESTIMATION RMSE.

$W$	$k_m^i$ [MPa/m]	$b_m^i$ [MPa/(m·s <sup>-1</sup> )]	$k_m^w$ [MPa/m]	$b_m^w$ [MPa/(m·s <sup>-1</sup> )]	$\alpha$ [MPa]	$\beta$	$\sigma_y$ [KPa]	$\zeta$	$\omega_0$	RMSE [%]
15%	1.21	0.24	1.48	1.35	0.17	0.56	17	0.47	4.09	7.01
20%	0.70	0.16	1.71	1.56	0.12	0.49	14	0.31	3.45	5.82
25%	0.26	0.29	1.21	1.35	0.04	0.54	6	0.49	2.23	5.37
30%	0.11	0.06	1.27	1.40	0.01	0.46	2	0.36	1.44	4.09
35%	0.28	0.07	1.16	1.36	0.01	0.38	2	0.81	2.21	6.61

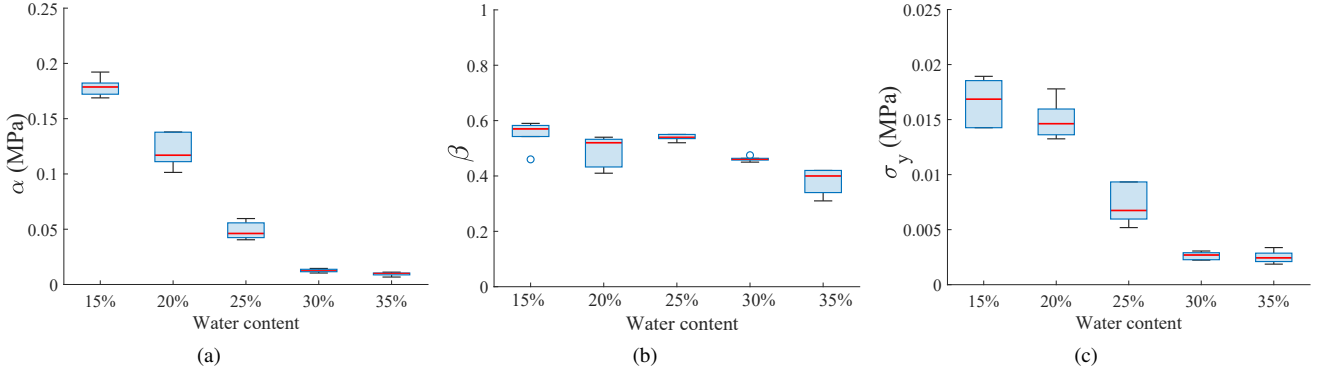


Fig. 7. Box plots of the estimated parameter values for mud with various water content. (a) Stiffness parameter  $\alpha$ . (b) Stiffness parameter  $\beta$ . (c) Mud yielding threshold  $\sigma_y$ . The blue box indicates min-max values and quartiles. The red line indicates the median value.

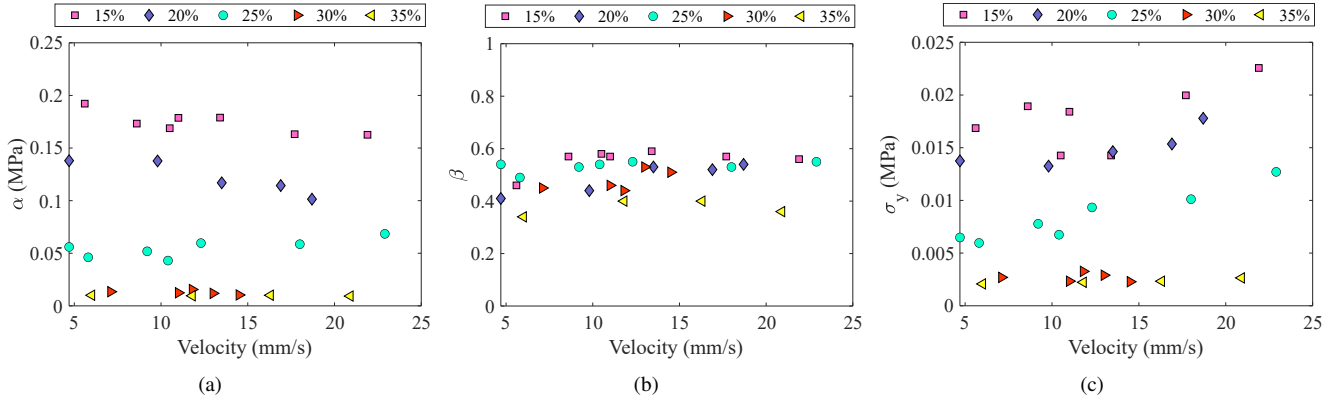


Fig. 8. Estimated parameter values at various intrusion velocity  $\dot{z}_i$ . (a) Stiffness parameter  $\alpha$ . (b) Stiffness parameter  $\beta$ . (c) Mud yielding threshold  $\sigma_y$ .

force and  $\beta$  however generally decreases slightly as shown in Figs. 7(a) and 7(b). Fig. 7(c) shows that with a high water content, the value of the yield stress  $\sigma_y$  becomes small, implying that the mud becomes flowable but less cohesive and is unable to provide significant suction force before material necking happens. Figs. 8(a) and 8(b) show the model parameters  $\alpha$  and  $\beta$  under various intrusion velocities. For the same water content, the magnitudes of  $\alpha$  and  $\beta$  are relatively constant. Yield stress threshold  $\sigma_y$  determines when necking happens and the suction force starts reducing. Unlike  $\alpha$  and  $\beta$ , yield stress threshold  $\sigma_y$  might be influenced by the withdrawing motion velocity. Fig. 8(c) shows the relationship between  $\sigma_y$  and the withdrawal velocity. It is interesting to see that for  $W = 15, 20,$  and  $25\%$ , the value of  $\sigma_y$  slightly increases along with the increasing velocity  $\dot{z}_i$ , while it remains almost constant at high  $W = 30$  and  $35\%$ . We also conducted intrusion experiments on mud and dry/wet sand for comparisons. For both mud and wet sand, the water content was set as  $W = 25\%$ . Fig. 9 shows

the comparison experiments of the foot-sand and foot-mud resistive force results. It is clear that the presence of visco-elasticity (damping) effect was obvious during late intrusion and sustain process for mud. In the sustain regime, the mud resistive force magnitude demonstrated obvious relaxation and decayed to a steady value. However, the dry/wet sand showed a linearity approximately during the intrusion process and almost no relaxation. Furthermore, no suction force was observed for dry/wet sand. This overall nonlinearity of mud stiffness and significant cohesion/suction property made the RFT force models for sand not applicable for mud terrain.

It is difficult to describe and predict the quantitative relationship between water content and model parameters since it highly depends on mud ingredients. For the mud with high water content and flowability, the cohesion of mud becomes insignificant so that yield stress is small and necking easily happens. By differentiating the curve in Fig. 7(c) with respect to  $W$ , we can find a critical stress after which mud becomes flowable. Therefore, it is feasible to use this threshold stress

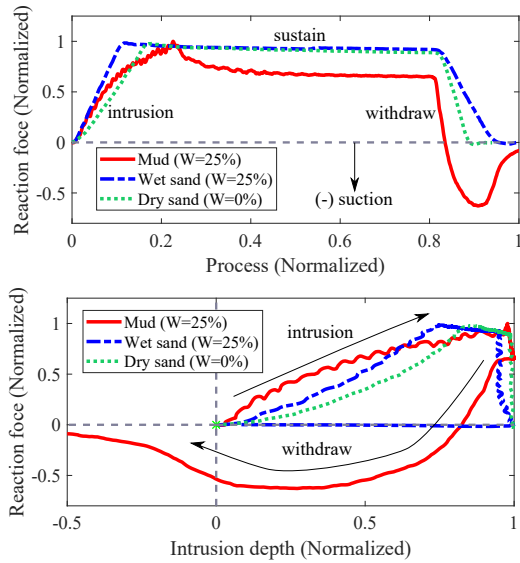


Fig. 9. The normalized reaction force comparisons on mud and dry/wet sand media. Top: force profiles in time domain. Bottom: force profiles over the intrusion process.

to identify the mud rheological characteristics and design the locomotion gait strategies.

This work found that an increase of water content from 15 to 35% reduced the resistive force significantly, which is implied from the decreasing trends of mud stiffness  $k_m^i$  ( $k_m^w$ ) and  $\alpha$ ; see Figs. 6 and 7(a). Similar results were reported in [15], [16]. However, the previous findings were obtained empirically while the results in this paper provide modeling analysis with physical interpretation. The proposed model used the foot velocity as input to directly estimate resistive force instead of solving constitutive equations to predict shear rate and shear stress as in [11]–[13], which were difficult to obtain in real time for robotic applications.

Although the proposed model predicted the mud reaction force accurately, the foot locomotion was considered as a simple vertical intrusion motion. It is necessary to extend this one-dimensional model for to arbitrary three-dimensional (3D) robotic foot locomotion. We only showed a case study on the parametrical dependency on water content rather than developing a physically informative model to interpret experimental observations and to infer underlying physics. We are seeking to overcome these limitations as part of future research directions.

## V. CONCLUSIONS

We presented a reduced-order model for interactions between robot and muddy terrain. We first conducted mud intrusion experiments and highlighted corresponding foot-mud interaction force characteristics. A visco-elasto-plastic analog was used to infer underlying physical mechanism for resistive force estimation. This model took both the intrusion and withdrawing suction into consideration and integrated the foot motion into the mud rheological response directly. Through experiments, the proposed model was evaluated under different water content and motion conditions. An ongoing effort is to extend the 1D reaction force model to 3D

foot motion applications for legged robots. Integration of the foot-mud interactions with bipedal balance control (e.g., [19], [20]) is another ongoing research direction.

## REFERENCES

- [1] J. Aguilar, T. Zhang, F. Qian, M. Kingsbury, B. McInroe, N. Mazouchova, C. Li, R. Maladen, C. Gong, M. Travers, R. L. Hatton, H. Choset, P. B. Umbanhowar, and D. I. Goldman, "A review on locomotion robophysics: The study of movement at the intersection of robotics, soft matter and dynamical systems," *Rep. Prog. Phys.*, vol. 79, 2016, article 110001.
- [2] S. Godon, M. Kruusmaa, and A. Ristolainen, "Maneuvering on non-newtonian fluidic terrain: a survey of animal and bio-inspired robot locomotion techniques on soft yielding grounds," *Front. Robot. AI*, vol. 10, 2023, article 1113881.
- [3] C. Li, T. Zhang, and D. I. Goldman, "A terradynamics of legged locomotion on granular media," *Science*, vol. 339, no. 6126, pp. 1408–1412, 2013.
- [4] L. Huang, J. Zhu, Y. Yuan, and Y. Yin, "A dynamic resistive force model for designing mobile robot in granular media," *IEEE Robot. Automat. Lett.*, vol. 7, no. 2, pp. 5357–5364, 2022.
- [5] S. Jung, A. G. Winter, and A. Hosoi, "Dynamics of digging in wet soil," *Int. J. Nonlinear Mech.*, vol. 46, no. 4, pp. 602–606, 2011.
- [6] T. M. Huh, C. Cao, J. Aderibigbe, D. Moon, and H. S. Stuart, "Walk-burrow-tug: Legged anchoring analysis using rft-based granular limit surfaces," *IEEE Robot. Automat. Lett.*, vol. 8, no. 6, pp. 3796–3803, 2023.
- [7] X. Chen, J. Yi, and H. Wang, "Energy efficient foot-shape design for bipedal walkers on granular terrain," *IFAC-PapersOnLine*, vol. 56, no. 3, pp. 601–606, 2023.
- [8] X. Chen, A. Anikode, J. Yi, and L. Tao, "Foot shape-dependent resistive force model for bipedal walkers on granular terrains," in *Proc. IEEE Int. Conf. Robot. Autom.*, Yokohama, Japan, 2024, <https://doi.org/10.48550/arXiv.2403.03460>.
- [9] T. Hossain and P. Rognon, "Drag force in immersed granular materials," *Phys. Rev. Fluids*, vol. 5, no. 5, 2020, article 054306.
- [10] P. Coussot and J. M. Piau, "On the behavior of fine mud suspensions," *Rheol. Acta*, vol. 33, pp. 175–184, 1994.
- [11] L. Bocquet, A. Colin, and A. Ajdari, "Kinetic theory of plastic flow in soft glassy materials," *Phys. Rev. Lett.*, vol. 103, no. 3, 2009, article 036001.
- [12] M. Caggioni, V. Trappe, and P. T. Spicer, "Variations of the herschel-bulkley exponent reflecting contributions of the viscous continuous phase to the shear rate-dependent stress of soft glassy materials," *J. Rheol.*, vol. 64, no. 2, pp. 413–422, 2020.
- [13] R. Ran, S. Pradeep, S. Kosgodagan Acharige, B. C. Blackwell, C. Kammer, D. J. Jerolmack, and P. E. Arratia, "Understanding the rheology of kaolinite clay suspensions using bayesian inference," *J. Rheol.*, vol. 67, no. 1, pp. 241–252, 2023.
- [14] X. Ren, X. Liang, Z. Kong, M. Xu, R. Xu, and S. Zhang, "An experimental study on the locomotion performance of elliptic-curve leg in muddy terrain," in *Proc. IEEE/ASME Int. Conf. Adv. Intell. Mechatronics*, Wollongong, Australia, 2013, pp. 518–523.
- [15] S. Liu, B. Huang, and F. Qian, "Adaptation of flipper-mud interactions enables effective terrestrial locomotion on muddy substrates," *IEEE Robot. Automat. Lett.*, vol. 8, no. 12, pp. 7978–7985, 2023.
- [16] S. Godon, A. Ristolainen, and M. Kruusmaa, "An insight on mud behavior upon stepping," *IEEE Robot. Automat. Lett.*, vol. 7, no. 4, pp. 11 039–11 046, 2022.
- [17] F. Q. Potiguar and Y. Ding, "Lift and drag in intruders moving through hydrostatic granular media at high speeds," *Phys. Rev. E*, vol. 88, no. 1, 2013, article 012204.
- [18] A. Shakeel, A. Kirichek, and C. Chassagne, "Yield stress measurements of mud sediments using different rheological methods and geometries: An evidence of two-step yielding," *Mar. Geol.*, vol. 427, 2020, article 106247.
- [19] M. Mihalec, M. Trkov, and J. Yi, "Balance recoverability and control of bipedal walkers with foot slip," *ASME J. Biomech. Eng.*, vol. 144, no. 5, 2022, article 051012.
- [20] M. Mihalec and J. Yi, "Balance gait controller for a bipedal robotic walker with foot slip," *IEEE/ASME Trans. Mechatronics*, vol. 28, no. 4, pp. 2012–2019, 2023.